



Numerical Analysis of Thermal Cracking Estimation of Mass Concrete With Ggbs at an Early Age

Moustafa A. Shawkey^{a,*}, Ahmed M. Hassan^b, Mohamed M. Rashad^c



CrossMark

^aEnvironmental Sciences and Industrial Development Department, Faculty of Postgraduate Studies for Advanced Sciences (PSAS), Beni-Suef University, Beni-Suef 62511, Egypt.

^bCivil Engineering Department, Faculty of Engineering, Beni-Suef University, Beni-Suef 62511, Egypt.

^cCentral Metallurgical Research and Development Institute (CMRDI), Helwan, Cairo 11421, Egypt.

Abstract

At an early age, the temperature rise in mass concrete is attributable primarily to the propagation of heat due to an exothermic reaction of cementitious materials and water. The temperature variation in the mass concrete between the core and its surfaces results in the development of thermal stresses. It might occur cracking if these stresses surpass the gained tensile strength of concrete. The paper compares experimental and numerical outcomes of heat generation in concrete mould $0.15 \text{ m} \times 0.15 \text{ m} \times 0.15 \text{ m}$ in size. Four concrete mixtures with ground granulated blast-furnace slag (GGBS) replacement to cement 0%, 10%, 30%, and 50% were used in the study. Virtual Cement and Concrete Testing Laboratory (VCCTL) software was used for obtaining the degree of hydration and adiabatic temperature of the four mixtures. Finite element modeling of these mixtures observed good agreement with experimental testing captured by the thermometer. Following that, numerical simulation was utilized to study the effect of the block size (cubic models with edge length 0.5 m, 1.0 m, 2.0 m, and 3.0 m) on temperature rise and the associated risk of cracking in mass concrete blocks.

Keywords: Early-age concrete; Thermal stress; Cracking.

1. Introduction

When vast amounts of concrete are poured during the construction of immense structures such as dams, bridges, and deep foundations, the quantity of heat of hydration obtained is considerable and should be taken into account [1]. Hydration of concrete is an exothermic reaction that produces a lot of heat during the first few days of hydration. Due to the insulating influence of the concrete, heat production can result in high temperatures at the core of the mass concrete [2]. Therefore, temperature gradients happen because the concrete surface temperatures are lower due to heat dissipation into the ambient environment [3]. The temperature variations between the structure's core and surface cause volumetric changes, such as heating expansion and cooling contraction [4]. Furthermore, tensile stresses form on the surface of the concrete when the supports restrain these volumetric variations. Moreover, at the early

age of the concrete structure, cracking usually occurs when the surface tensile stresses exceed the overall tensile strength of the concrete. Cracking is accentuated even more at an early age that is still developing its full strength [5].

Many researchers who created numerical models to estimate temperature variation in mass structures mainly used basic functions of heat generation to calculate adiabatic temperature rise [6]. Moreover, calculating heat generation by calorimetry measurements is uncommon in many developing countries because of the high cost of acquiring these instruments. That is why the importance of using alternative methods came to allow the institutions in these countries to forecast temperature distribution. This helps to explore other findings, such as framework demolding time and surface area to volume ratio (SVR) that may cause thermal cracks.

The influence of thermal differentials on mass

*Corresponding author e-mail: moustafa.shawkey@psas.bsu.edu.eg; (Moustafa A. Shawkey).

Receive Date: 23 September 2021, Revise Date: 13 November 2021, Accept Date: 18 November 2021

DOI: 10.21608/ejchem.2021.97424.4554

©2022 National Information and Documentation Center (NIDOC)

concrete is well understood, yet there is no consensus on the maximum temperature difference between a concrete structure's center and surface. The thermal behaviour of hydrated mass concrete has been successfully predicted by Bobko et al. [7], who set the temperature differential at 20°C. Numerous concrete institutions have formed their criteria in their countries to govern and limit the adverse effects of thermal cracking in mass concrete based on the location and time of such large concrete projects. This indicates that heat generation in mass concrete constructions differs in hot and cold regions [8].

Thermal stresses that happen during mass concrete maturity are exceedingly complex and challenging to quantify. This is due to several causes, the most important of which is the complex distribution of temperature variations throughout the mass concrete volume. At an early age, the temperature in the middle region of the mass concrete is high but uniform, whereas the temperature in the outer part is lower [9]. Due to concrete maturation and strength being temperature-dependent, the concrete structure's core gains more strength than in the external regions. High heat gradients are created when the concrete hydrates quicker in the core, and strength and hydration propagation decrease by moving towards the surface. Tensile stresses and strains will emerge due to resisting the contraction, perhaps resulting in cracks at or near the concrete's surface [10]. The values of the tensile stresses are influenced by several factors such as elastic modulus, degree of restraint, and thermal expansion [11]. The propagation of formed cracks affects the concrete structure's ability to withstand design loads and allow harmful elements to infiltrate the mass concrete construction, jeopardizing its integrity and durability [12].

Supplementary cementitious materials (SCM) such as fly ash (FA) and ground granulated blast-furnace slag (GGBS) are frequently used in concrete mixtures to substitute a portion of the Portland cement. When a large percentage of FA or GGBS is used to replace cement, the heat of hydration generated in the concrete is reduced, followed by lower tensile strength at an early age. Many trials have been carried out to reduce the heat generation and in parallel achieve a reasonable mechanical strength [13-15].

The current paper displays a comparison between

experimental and numerical monitoring of the temperature of concrete with different GGBS ratios, 0%, 10%, 30%, and 50%. Finite-element modeling of the heat of hydration obtained from VCCTL software was used to predict these models' temperature variation and thermal stresses. Numerical modeling was subsequently used to identify the effects of the size of the structure using different GGBS ratios on the maximum temperature and thermal stresses in the mass concrete blocks to evaluate cracking possibilities.

2. Experimental setup

2.1. Materials and mix proportion

Concrete samples in the study were prepared using a Portland Cement CEM I (42,5 N), Elaskary Cement-BeniSuef, manufactured by National company for cement (NCC), Egypt to match with the physical property and chemical composition requirements released in the Egyptian Standard Specifications (ES 4756-1/2013) that technically identical with the British Standards Institution (BS EN 197-1:2011) [16]. In addition, Ground Granulated Blast-furnace Slag (GGBS) was used in the samples with various ratios to cement, shown in Figure 1. Table 1 displays the main constituent properties of cement [17] and GGBS used in this study. Cement, GGBS, gravel, sand, and tap water were used to form four mixes of concrete with w/c 0.45 and by changing GGBS weight percentages to be 0% (G0), 10% (G10), 30% (G30), and 50% (G50), respectively, Table 2 displays mix designs of concrete samples used in the study. Four Cubic moulds with an edge length of 150 mm for thermal analysis, and 12 moulds with an edge length of 100 mm for compressive testing were made to form concrete samples, shown in Figure 2. The samples were mixed and casted in moulds at initial temperature 30 °C and the average temperature during the next 72 h was 27 °C.

Table 1. Main constituent properties of cement and GGBS

Mix no.	SiO ₂	Al ₂ O ₃	Fe ₂ O ₃	CaO	MgO	SO ₃	K ₂ O	Na ₂ O
Cement	20.38	4.77	3.75	62.44	1.25	2.53	0.23	0.43
GGBS	42.01	13.36	0.52	33.96	4.47	1.63	0.81	1.98



Figure 1. Materials used in the study Cement; (b) GGBS



Figure 2. Cubic samples (10 cm³) for the four mixtures of concrete

2.2. Thermal measurement setup

K-type thermocouples were embedded in concrete moulds' core (that obtain the maximum temperature) right after casting to record internal temperature changes in hydration heat until 72 h of hydration. Temperature results were captured continuously at every 4 min using an HH-520 4-channel thermocouple data logger. The thermocouples results were obtained at various time intervals to validate the proposed finite element model for identifying the potential for cracks occurring at early age of concrete. Figure 3 explains the setup of the thermal experiment. *Mechanical properties of concrete*

The determining of compressive and tensile strength of concrete is vital to evaluate early-age stress analysis of samples, by comparing the tensile strength with the tensile stress resulted from the proposed modeling of concrete [18]. Many equations to predict the compressive strength of concrete have been provided. Two familiar used equations are shown in Equations (1) and (2)[2]:

$$f_{c,t} = a + b \log(\log(M(t))) \quad (1)$$

$$f_c(t_c) = f_{c,ult} \cdot \exp\left(-\left(\frac{t_c}{T_e}\right)^{\beta_s}\right) \quad (2)$$

Where f_c is the compressive strength of concrete (MPa), a is a parameter that is always negative (MPa), b is a parameter (MPa^oC/h), $f_{c,ult}$ is the ultimate compressive strength of concrete (MPa), τ is a parameter (h), T_e is equivalent age at the curing temperature (h), β_s is a parameter, $M(t)$ is the maturity of concrete at age t , t_c is temperature of concrete during the time interval, t is time (h). In our study, compressive strength experiment was carried out after 28 days for the four mixtures, as described in Figure 4.

The authors provided many equations to estimate the tensile strength of concrete with respect to time intervals. One of these methods showed a power type function depends on the compressive strength[2]:

$$f_{i,28} = a (f_{c,28})^b \quad (3)$$

where $f_{i,28}$ is the concrete tensile strength of concrete at 28 days, a and b are parameters, and $f_{c,28}$ is the compressive strength of concrete at 28 days. It was found that values of parameters a and b were 0.06 and 1.09, respectively. To predict the tensile strength of concrete over time until 28 days, the following equation was provided[19]:

$$f_{i,t} = (1 + 0.3 \log(t/28))^{0.716} f_{i,28} \quad (4)$$

Where $f_{i,28}$ is the concrete tensile strength of concrete over time interval t , t is the time (h).

2. Table 2. Mix designs of concrete samples used in the study

Mix no.	Cement (Kg/m ³)	GGBS (Kg/m ³)	GGBS/Cement Ratio	gravel (Kg/m ³)	Sand (Kg/m ³)	W/C Ratio	Water (L/m ³)
G0	500	0	0 %	1031	740	0.45	225
G10	450	50	10 %	1031	740	0.45	225
G30	350	150	30 %	1031	740	0.45	225
G50	250	250	50 %	1031	740	0.45	225

2.4. Scanning Electron Microscopy

The qualitative analysis of concrete mixtures was conducted by Field Emission Scanning Electron Microscopy (FE-SEM) is beneficial for a better understanding of hydration products after 28 days of hydration. The morphology and elemental distribution analysis of the concrete samples were carried out by (Zeiss Sigma 500 VP Analytical FE-SEM). The used detector was (Secondary Electron (SE) Detector), and the operating voltage was kept at 10 to 12 kV.

2.5. Numerical analysis method

The Fourier heat transfer equation is a mathematical model for calculating the temperature of an elemental volume at a specific time. In the three-dimensional heat flow analysis, the following generalized governing Equation was used [20].

$$\rho C_P \frac{\delta T}{\delta t} = K \left(\frac{d^2 T}{dx^2} + \frac{d^2 T}{dy^2} + \frac{d^2 T}{dz^2} \right) + Q_H(5)$$

Where ρ is the density of concrete, K is the concrete thermal conductivity that expresses the heat transfer rate because of the temperature gradient concrete; T is the temperature, which is the internal heat generation rate of concrete, C_P is the specific heat of concrete, indicates the amount of absorbed energy to raise the concrete temperature; t is the time and x , y , and z are the axes of coordinate, and Q_H is the heat generation per unit volume. The assumed values of parameters used in the simulation are obtained in Table 3. Virtual Cement and Concrete Testing Laboratory (VCCTL) is compelling, three-dimensional software for simulating mechanical and hydration properties of concrete based materials over time. The principle of VCCTL simulation is established upon the technology of NIST microstructure and software of CEMHYD3D hydration. VCCTL includes important information regarding the chemical and physical behavior of concrete. The capabilities of VCCTL reached to forecast behaviors of concrete with supplementary cementitious materials such as silica fume, GGBS, and fly ash. The previous references explained an acceptable matching between the simulated and experimental data. However, the input parameter of elements included in the mix such as cement, water, fine and coarse aggregate, and supplementary

materials should be as accurate to obtain precise forecasting [9].

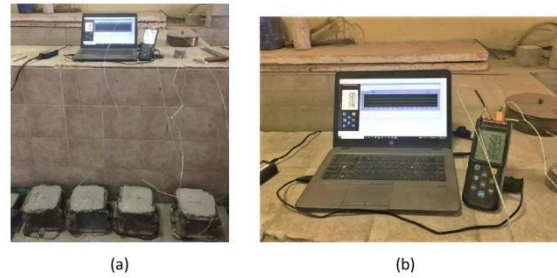


Figure 3. (a) Experimental setup; (b) Photograph displaying data logger thermometer



Figure 4. Compression test of concrete samples

A finite element modeling (FEM) of a cubic concrete with dimensions $0.15 \text{ m} \times 0.15 \text{ m} \times 0.15 \text{ m}$ was built using ANSYS Workbench software. The model was established to estimate, firstly, the heat of hydration of concrete's core during the first 72 h of hydration. The Transient Thermal and Transient Structural Analysis systems were used in this simulation. For such problems, the FEM analysis is very satisfactory and widely used for getting accurate data. A meshing of 8 mm of minimum edge length was used in this study to achieve good estimates of the temperature distribution, was shown in Figure 5.

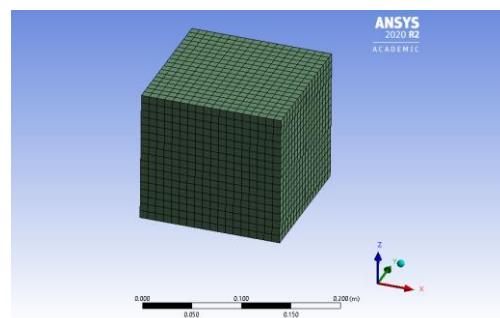


Figure 5. Modeling of thermal and stress analysis for concrete samples

Table 3. Execution parameters used for thermal and stress analysis

Parameters	Units	value
Thermal conductivity	W/m °C	2.5
Specific heat	J/kg/°C	960
Density	Kg/m ³	2400
Convection - air	W/m ² °C	5
Convection - steel	W/m ² °C	14
Coefficient of Thermal Expansion	/°C	8 E-06
Young's Modulus	GPa	28.1
Poisson's Ratio		0.17
Initial ambient temperature	°C	30
Average ambient temperature	°C	27
Analysis time	h	72 & 120

After achieving the modeling validation, another series of simulation modeling for the four mixtures were carried out. Cubic models with length edge 0.5 m, 1.0 m, 2.0 m, and 3.0 m were proposed to show the maximum internal temperature of concrete. Moreover, the cracking behavior of the concrete was simulated by obtaining the tensile stress of the models at the upper surface, which shows the maximum value of tensile stress.

Cracking in concrete appears when the tensile stresses of concrete exceed the tensile strength. The crack index of concrete is obtained according to the following equation [13]:

$$I_{cr,t} = f_{ts,t} / f_{t,t} \quad (6)$$

Where $I_{cr,t}$ is the crack index, $f_{ts,t}$ is the thermal stresses of concrete and $f_{t,t}$ is the tensile strength of concrete. When the crack index approaches or exceeds 1, which means the cracks start to generate.

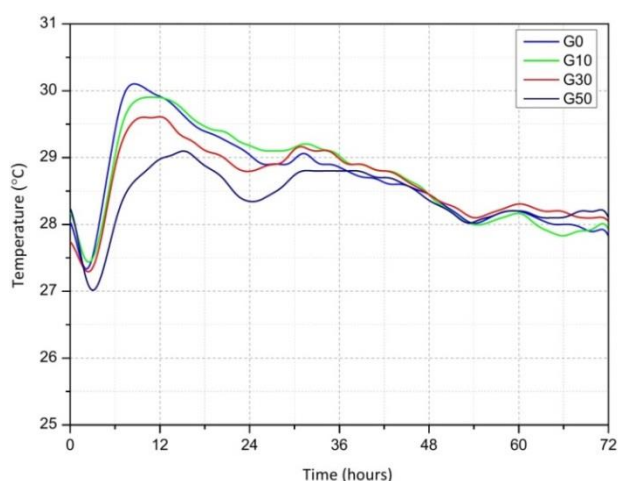


Figure 6. Temperature rise at the core of concrete samples during 72 h of hydration

3. Results

3.1. Temperature measurement results

Internal heat in concrete samples measured using a thermocouple data logger is considered an indicator of hydration development. The propagation of the hydration process was significantly linked to the exothermic hydration response induced by a change in internal temperature. Figure 6 shows the experimental change in internal temperature as a function of time at the center of concrete samples G0, G10, G30, and G50 during the first 72 h of hydration. The four samples have the same behavior, as the temperature decreased for a short time and then jumped rapidly until they reached the maximum values. The peak temperatures recorded at the center in the concrete samples in the field were 30.1 °C at 8.5 h, 29.9 °C at 10.9 h, 29.6 °C at 12.0 h, and 29.1 °C at 15.2 h for samples G0, G10, G30, and G50, respectively. The results confirmed the previous references that concrete samples with a lower GGBS ratio reach higher peak temperatures than a higher ratio due to GGBS having a considerable slow rate of hydration reaction [13].

3.2. VCCTL results

Figure 7,b shows the degree of hydration curve conducted by VCCTL simulation for the concrete mixtures during 120 h of hydration. The concrete mixtures' adiabatic Temperature Rise (ATR) was also obtained using VCCTL software in Figure 7,a. It was observed that the degree of hydration at 120 h reached 84%, 83%, 81%, and 75% for mixtures G0, G10, G30, and G50, respectively. Moreover, according to adiabatic temperature, The mixs' initial temperature stated at 28 °C, and the temperature rise during the 120 h testing period reached 96 °C, 91 °C, 79 °C, and 63 °C for mixtures G0, G10, G30, and G50, respectively. The simulated ATR curve was

obtained and used to describe the concrete heat of hydration; it served as the base for the thermal loading function in the thermal analysis. It was the first stage of simulation, and the data of adiabatic temperatures would pass to the ANSYS workbench to estimate the hydration temperature for the different mixtures. The more GGBS percentage in the concrete mix, the lower the hydration rate exhibited, and thus the lower the adiabatic temperature value. The heat transfer in concrete starts from the thermal energy released during the cement hydration process. The heat of hydration rate depends not only on the concrete mixture itself but also on the initial concrete temperature, temperature histories, formwork type, and wind velocity [2]. The thermal loading can vary between two identical concrete structures cast in two different temperature environments.

3.3. Temperature rise comparison: experimental and numerical

The finite element model was used to estimate temperature change in each monitored concrete structure of G0, G10, G30, and G50. The computed temperatures obtained from the finite element model were then evaluated with the captured temperatures by thermal testing. Each finite model of the concrete mixture had different boundary conditions to be analyzed. The internal temperatures of concrete mixtures at the core measured in the lab were compared to the simulated temperatures during the first 72 h of hydration. Figure 8 shows the internal temperatures of the experimental and simulated concrete mixtures of G0, G10, G30, and G50.

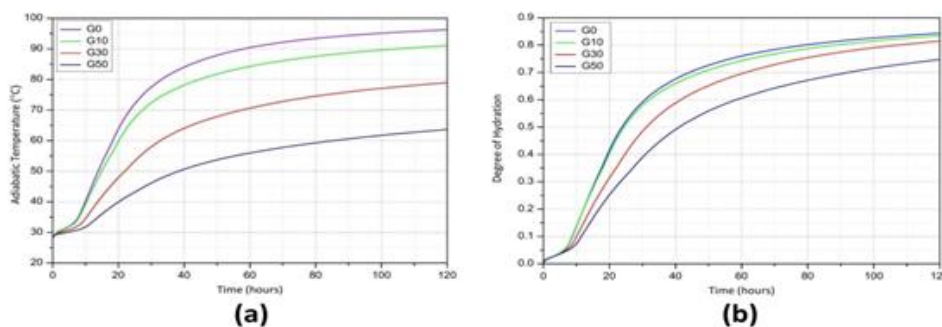


Figure 7. VCCTL analysis of concrete samples during 120 h of hydration, (a) adiabatic temperature (b) degree of hydration

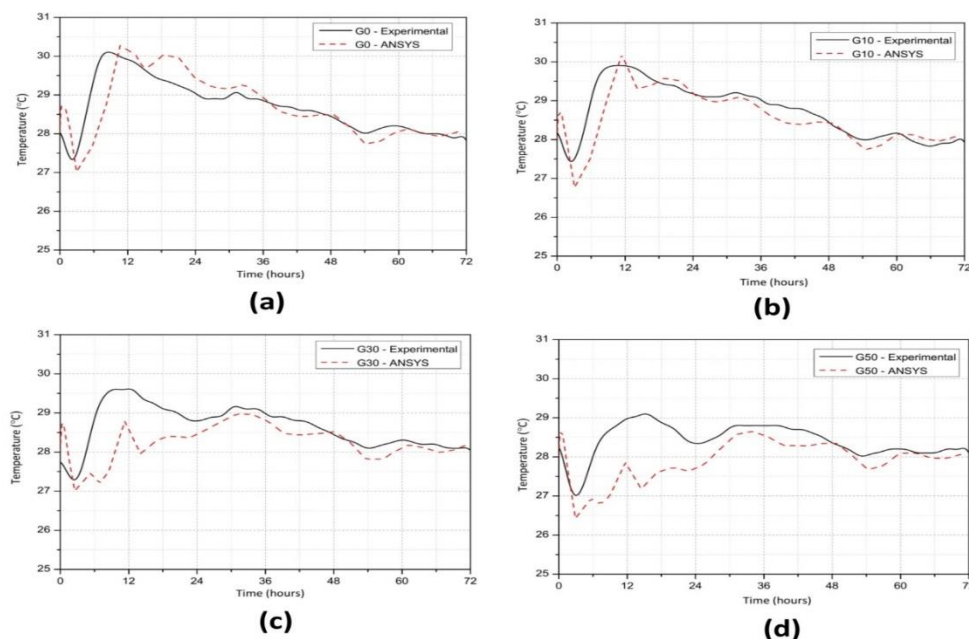


Figure 8. Temperature variation at the core of concrete samples with respect to time during the first 72 h of hydration, (a) G0 (b) G10 (c) G30 and (d) G50

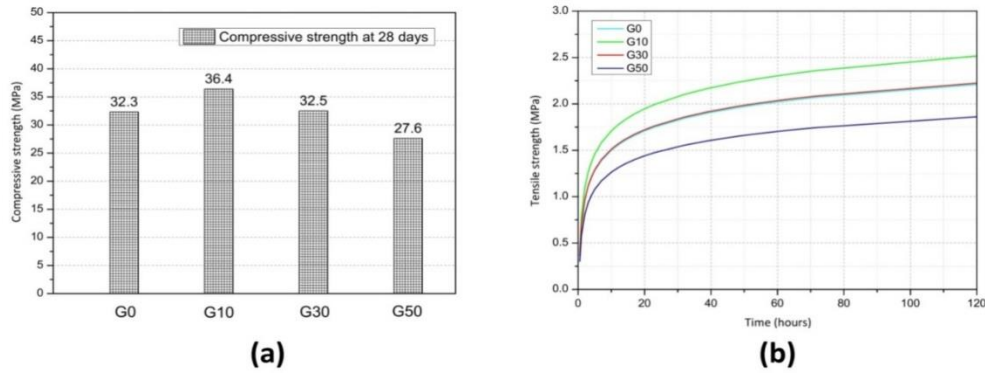


Figure 9. Mechanical properties of concrete samples, (a) compressive strength at 28 days (b) tensile strength over time

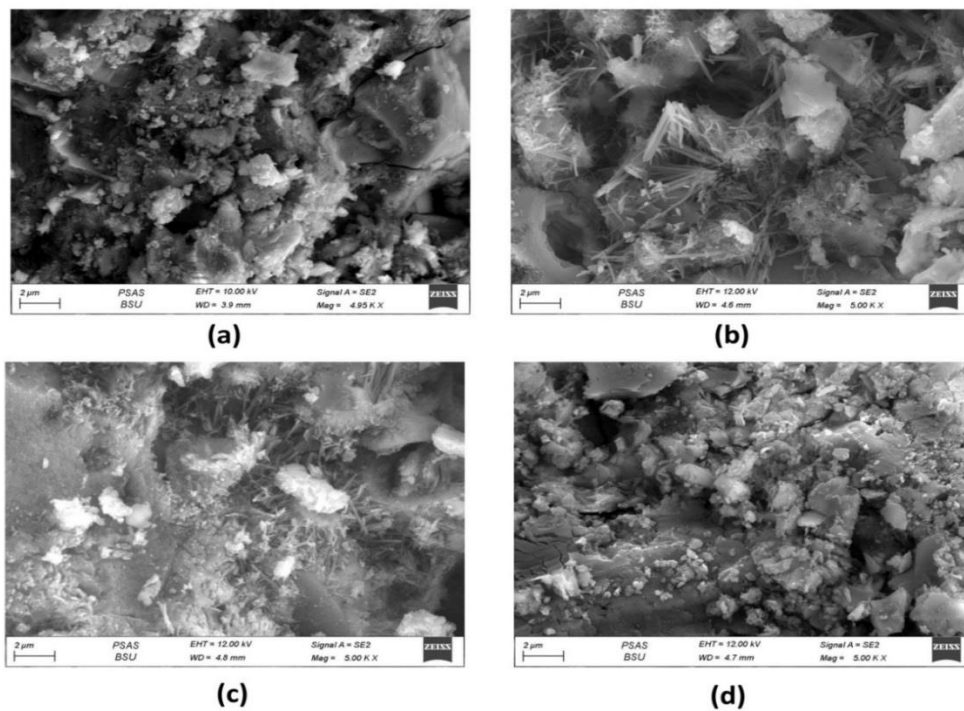


Figure 10. SEM photographs of concrete samples after 28 days of hydration, magnification 5 000 x, (a) G0 (b) G10 (c) G30 and (d) G50

A 30.3 °C temperature rise at 10.7 h was observed at the core of the simulated concrete mixture G0, Compared to the actual results obtained (30.1 °C at t = 11.4 h). For mixture G10, the maximum FEM temperature obtained was 30.2 °C at 11.4 h. According to concrete mixture G30, the maximum simulated temperature was 29.0 °C at 30.8 h. the maximum temperature in mixture G50 reached 28.7 °C at 33.9 h. Figure 8 shows the concretes' temperature distributions representing the FEM peak of temperature: at 38445 s (10.7 h) for G0, at 41043 s (11.4 h) for G10, at 1.11e5 s (30.8 h) for G30, and 1.22e5 s (33.9 h) for G50.

From the previous explanations, it is notable that most of the temperatures predicted in the finite element model closely match the temperatures measured in the lab, and the time of peak temperature as well-matched the mixtures G0 and G10. However, the simulated time of maximum temperature for mixtures G30 and G50 occurred later than the times obtained from the thermometer data logger. Overall, the validation of the FEM models had been successfully achieved.

3.4. Mechanical properties: compressive and tensile strengths

The compressive strength of concrete samples at 28 days was obtained in Figure 9. It is shown the compressive strength gained the maximum value by replacement of GGBS with 10 % of cement. The strength values of the mixes were 32.3 MPa, 36.4 Mpa, 32.5 Mpa, and 27.6 Mpa for G0, G10, G30, and G50, respectively. This means the substitution of GGBS with a 10% increased decreased the strength by 13 %. However, 30% substitution decreased the strength until it reached a nearby value gained by the control sample. The 50% GGBS substitution also decreased the mechanical strength of concrete by 15%, explained in Figure 9, a.

According to tensile strength, the strength values (f_s) at 28 days are normally predicted by cubic compressive strength ($f_{cu,28}$), as shown in equation (1). The tensile strengths for mixtures G0, G10, G30, and G50 were 2.65 MPa, 3.02 Mpa, 2.67 Mpa, and 2.23 Mpa, respectively. Moreover, the tensile strength values throughout the time interval of 120 h are obtained in Figure 9,b by applying equation no. (4). these strengths will be used for the evaluation procedure of the crack index of mixtures. The progress of compressive and tensile strength of concrete reinforced with supplementary material might connect to the overall rate of hydration degree. Still, the morphology of these admixtures also has an important influence on the hydration products.

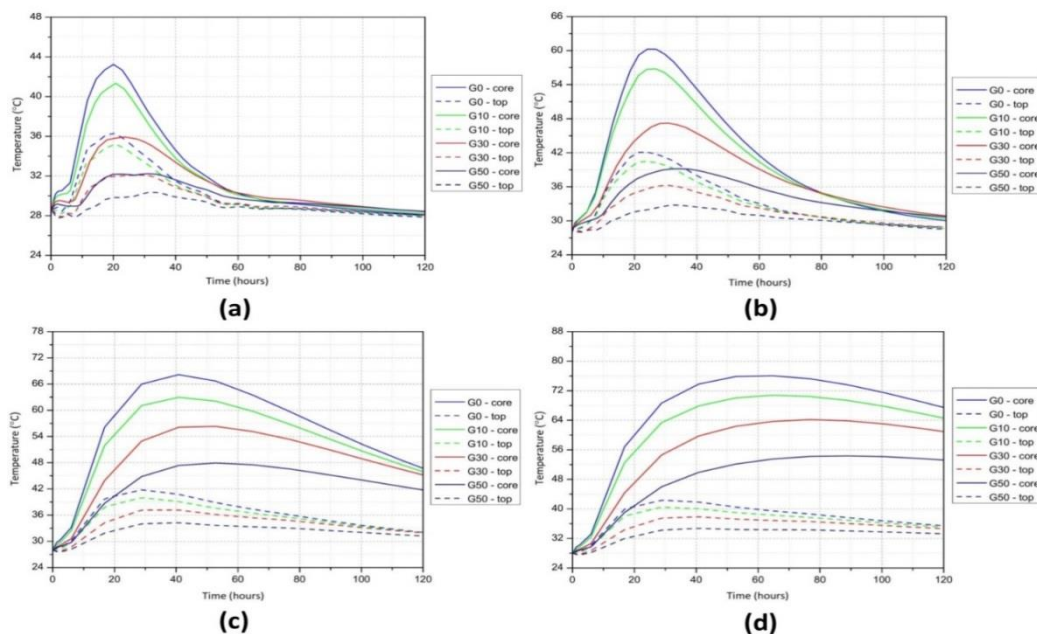


Figure 11. Temperature variation at the core and top surface for concrete mixtures (a) 0.5 m model (b) 1.0 m model (c) 2.0 m model (d) 3.0 m model

3.5. Scanning Electron Microscopy analysis

Figure 10 shows the SEM images of concrete with 0%, 10%, 30%, and 50% GGBS at 28 days. The figure shows clearly the cement hydration products of Portland cement, such as Calcium Silicate Hydrates (CSH), Calcium Hydroxide (CH), and Ettringite. Furthermore, the CSH gel (one of Portland cement's main hydration products) serves as a binder, holding the composites together [21]. From Figure 10,b, the addition of GGBS by 10 % Led to the morphology of

the binder's hydration products shown as more compact and generated interweaving thick needles (the calcium carbonate), which is responsible for the improvement of compressive and tensile strength. However, the 30% GGBS addition resulted in fewer sizes of needles, as shown in Figure 10,c, which gave an indication the strengths became lower compare to the G10 mixture. According to Figure 10,d, it is shown the absence of the needles and appearing of gabs through the image, which means a less compacted mix and lowers strength values. These

observations clearly matched with gained values compressive and tensile strengths.

3.6. temperature rise and thermal stresses at different sizes

After achieving a validation process for both VCCTL and ANSYS software and the simulated outcomes observed good agreement with experimental testing, another series of parametric studies had been conducted using ANSYS finite element program. The effects of structure size on peak temperature, temperature distribution, and generated stresses in mass concrete structures are examined.

The standard concrete model size used in the study was a block size of $0.15\text{m} \times 0.15\text{m} \times 0.15\text{m}$. To explore the effect of size on the thermal behaviour of concrete, four model sizes were simulated. The sizes chosen were $0.5\text{m} \times 0.5\text{m} \times 0.5\text{m}$, $1\text{m} \times 1\text{m} \times 1\text{m}$, $2\text{m} \times 2\text{m} \times 2\text{m}$, and $3\text{m} \times 3\text{m} \times 3\text{m}$. These models used the simulated adiabatic temperature rise curves of the concrete mixtures as a heat source. A comparison of the temperature profiles at the core and top center of models for the four mixtures G0, G10, G30 and G50 is shown in Figure 11. According to the control mixture (G0), as expected, the peak temperature increased as the model's size increased. It is shown that the temperature peaks for models were $43.1\text{ }^\circ\text{C}$, $60.3\text{ }^\circ\text{C}$, $67.7\text{ }^\circ\text{C}$, and $76.1\text{ }^\circ\text{C}$, while the temperature differential between the center and top surface increases by increasing sizes, $6.9\text{ }^\circ\text{C}$, $18.5\text{ }^\circ\text{C}$, $27.8\text{ }^\circ\text{C}$, $36.6\text{ }^\circ\text{C}$ for models 0.5 m , 1.0 m , 2.0 m , and 3.0 m , respectively.

Figure 12 displays the Ansys model for the temperature peak of the different sizes. The authors identified many factors that cause thermal cracking. The increased distance between the core and the surfaces of the big models makes the core approach fully adiabatic conditions due to a little heat loss is dissipated to the air [22]. To explain, for the $3\text{m} \times 3\text{m} \times 3\text{m}$ block, it can be shown from the curves that the heat dissipation at the core is very slow as compared to the $0.5\text{m} \times 0.5\text{m} \times 0.5\text{m}$ block, and heat remained for a longer period in the structure.

A significant peak temperature resulted in Delayed Ettringite Formation (DEF), which resulted in

potential cracking of the concrete blocks. Other contributing factors for the cracking development may include; cement content and high humidity conditions [1]. The maximum temperature at the core that exceeds $70\text{ }^\circ\text{C}$ for precluding the phenomenon of DEF, which occurred for the size 3.0 m ($76.1\text{ }^\circ\text{C}$). Other theories assumed the propagation of early cracking. The maximum temperature differential between the center and top surface should not exceed $20\text{ }^\circ\text{C}$ [2]; this situation appeared in the size models 2.0 m ($27.8\text{ }^\circ\text{C}$) and 3.0 m ($36.6\text{ }^\circ\text{C}$).

However, the induced stress at the top surface of the concrete block accurately expresses the potential occurrence of thermal cracking, as the stress increases as moving from the core towards the top of the blocks [5]. Figure 14 clarified the generated thermal stresses from different sizes and compared them with the thermal strength of the mixture G0. Notable notes that the strengths in all sizes override the permeable strength and Crack index exceed the value of 1 at specific time intervals; thus, cracking was expected to happen in these sizes.

Figures 11 and 13 display temperature peak, temperature surface, and temperature differences for all size models with different percentages of GGBS. A considerable decrease in temperature peak by increasing amount of GGBS in the concrete mix. The reduction ratio in temperature peak was from 4% to 7%, 16% to 22%, and 25% to 35% when the GGBS substitution was 10%, 30%, and 50%, respectively. Moreover, a notable decrease in the temperature difference is explained by increasing GGBS amount, which decreases the potential of cracks happening under maximum limits.

According to the thermal stresses of concrete with GGBS shown in Figures 14, 15, as previously mentioned, stresses for all size models for the control sample exceeded the allowable limits. Figure 15 displayed the reduction in stresses that led to decreasing stresses in the 0.5 m model (for G10, G30, and G50) to be lower than the strength. Furthermore, in Figure 15, b, stresses in model 1.0 m were significantly less than the strength of mix G30 and G50. However, Figure 15, c explained that the 2.0 m model for the same mixtures was very close to the strengths.

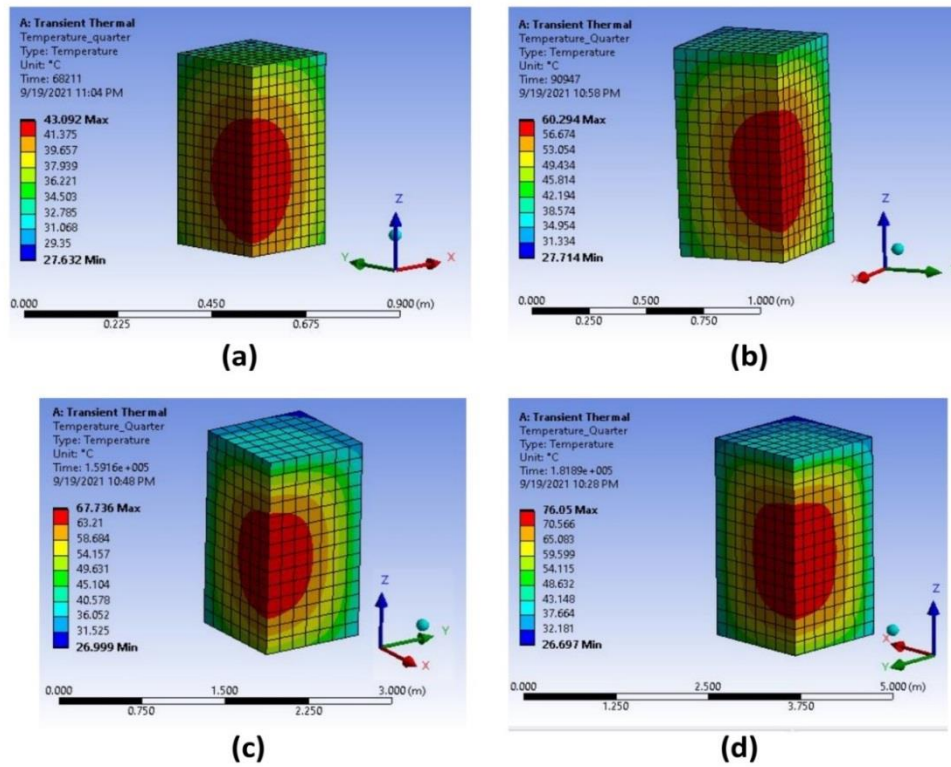


Figure 12. Temperature peak model for concrete mixture G0, (a) 0.5 m model (b) 1.0 m model (c) 2.0 m model (d) 3.0 m model

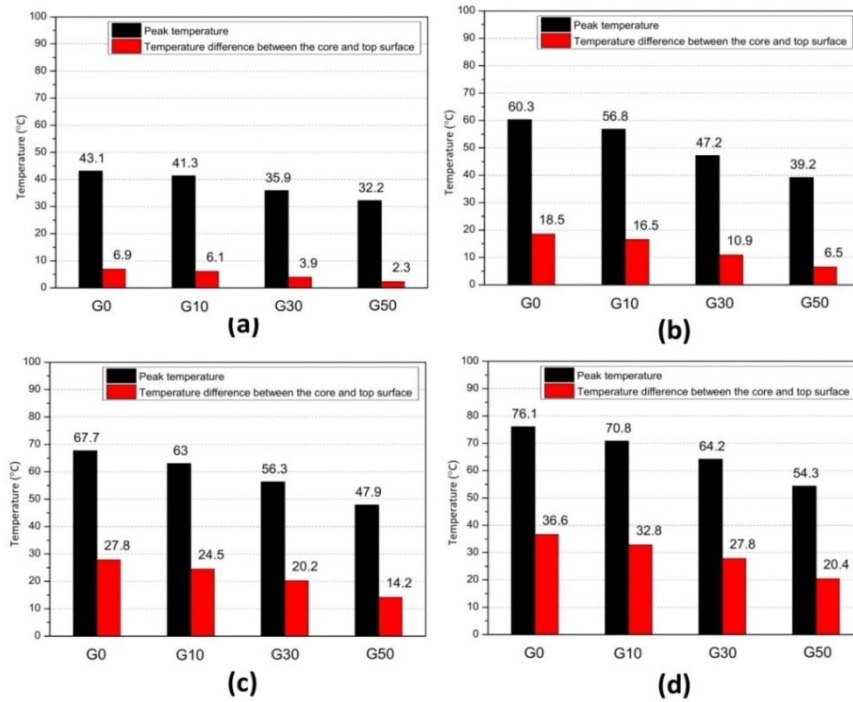


Figure 13. Peak temperatures and temperature difference between the core and top surface for concrete mixtures, (a) 0.5 m model (b) 1.0 m model (c) 2.0 m model (d) 3.0 m model

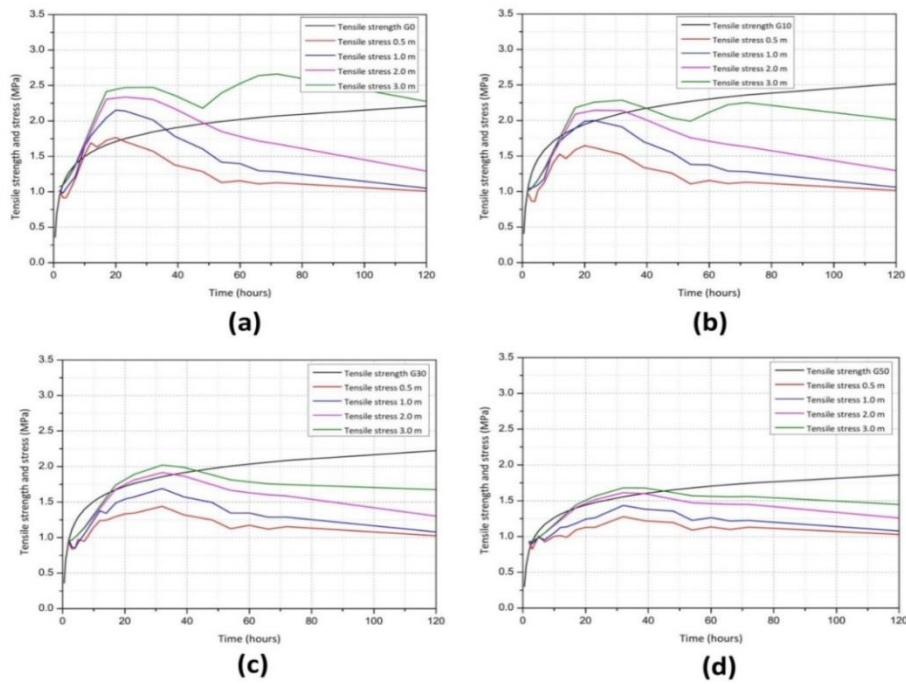


Figure 14. Tensile strength and stress of concrete samples, (a) G0 (b) G10 (c) G30 (d) G50

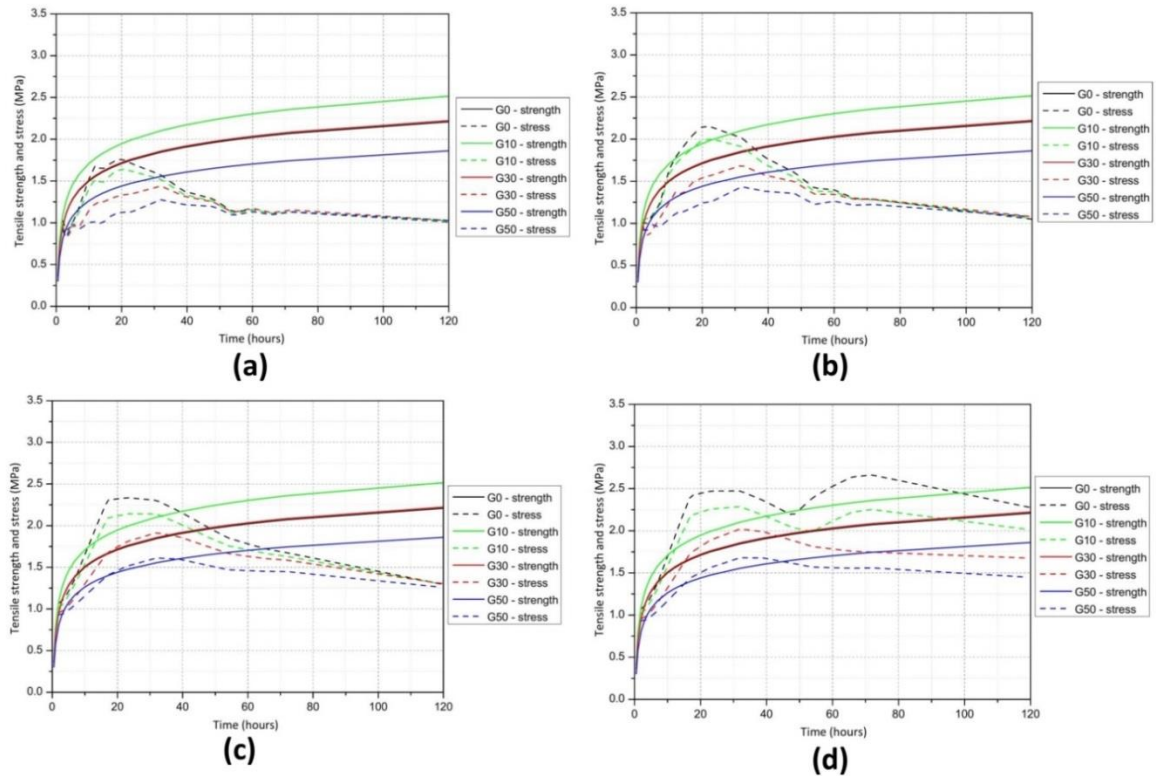


Figure 15. Tensile strength and stress of concrete samples, (a) 0.5 m model (b) 1.0 m model (c) 2.0 m model (d) 3.0 m model

4. Conclusion

In this paper, thermal testing was carried out during early age of concrete hydration. The purpose is to investigate the hydration process in concrete samples with different

GGBS/cement ratios. A comparison between experimental and numerical results of temperature variation at the core was identified. Moreover, another set of modeling investigations was executed, these

investigations aimed to precisely study the effect of changing sizes on the temperature rise and the possibility of cracking in mass concrete blocks. The findings are summed up as follows:

- 1- VCCTL software was a powerful method for predicting the thermal properties of concrete. The degree of hydration at 120 h slowed down by increasing GGBS amount, which approached 84%, 83%, 81%, and 75% for mixtures G0, G10, G30, and G50, respectively. However, the adiabatic temperature reached 96 °C, 91 °C, 79 °C, and 63 °C for the same mixtures.
- 2- Validation procedure had been achieved of the experimental and numerical results. The experiment and numerical temperatures were 30.1 °C and 30.3°C for mixture G0, 29.9 °C and 30.2 °C for mixture G10, 29.6 °C and 29.0 °C for mixture G30, and 29.1 °C and 28.7 °C for mixture G50, respectively.
- 3- The maximum compressive and tensile strength obtained by the replacement of GGBS to cement with 10 %, these results were confirmed by SEM.
- 4- The influence of decreasing thermal stresses by adding GGBS in concrete was crystal clear. For the different substitutions of GGBS, at models with sizes 0.5 m and 1.0 m, the stresses become below the thermal strengths. However, for models with sizes 2.0 m and 3.0 m, the stresses were decreased to reach close to the strengths.

5. References

- [1] B. A. Klemczak, "Modeling thermal-shrinkage stresses in early age massive concrete structures - Comparative study of basic models," *Arch. Civ. Mech. Eng.*, 2014, doi: 10.1016/j.acme.2014.01.002.
- [2] H. Abeka, S. Agyeman, and M. Adom-Asamoah, "Thermal effect of mass concrete structures in the tropics: Experimental, modelling and parametric studies," *Cogent Eng.*, vol. 4, no. 1, pp. 1–18, 2017, doi: 10.1080/23311916.2016.1278297.
- [3] A. Pofale, K. Tayade, and N. Deshpande, "Calorimetric Studies on Heat Evolution and Temperature Rise due to Hydration of Cementitious Materials in Concrete using Semi-," *Int. J. Appl. or Innov. Eng. Manag.*, vol. 2013, no. Ratmig, 2013.
- [4] K. A. Riding, J. L. Poole, K. J. Folliard, M. C. G. Juenger, and A. K. Schindler, "Modeling hydration of cementitious systems," *ACI Mater. J.*, vol. 109, no. 2, 2012, doi: 10.14359/51683709.
- [5] S.-G. Kim and K. Wang, "Effect of heat generation from cement hydration on mass concrete placement," *Civ. Eng.*, vol. Master of, 2010.
- [6] G. De Schutter, "Finite element simulation of thermal cracking in massive hardening concrete elements using degree of hydration based material laws," in *Computers and Structures*, 2002, vol. 80, no. 27–30, doi: 10.1016/S0045-7949(02)00270-5.
- [7] C. P. Bobko, A. J. Edwards, R. Seracino, and P. Zia, "Thermal Cracking of Mass Concrete Bridge Footings in Coastal Environments," *J. Perform. Constr. Facil.*, vol. 29, no. 6, 2015, doi: 10.1061/(asce)cf.1943-5509.0000664.
- [8] T. C. Nguyen and X. B. Luu, "Reducing temperature difference in mass concrete by surface insulation," *Mag. Civ. Eng.*, vol. 88, no. 4, 2019, doi: 10.18720/MCE.88.7.
- [9] K. J. Folliard et al., "Prediction model for concrete behavior - final report," *Texas Dep. Transp. Fed. Highw. Adm.*, vol. 7, 2008.
- [10] Y. Yuan and Z. L. Wan, "Prediction of cracking within early-age concrete due to thermal, drying and creep behavior," *Cem. Concr. Res.*, vol. 32, no. 7, 2002, doi: 10.1016/S0008-8846(02)00743-3.
- [11] N. T. Ho, T. C. Nguyen, A. K. Bui, and T. P. Huynh, "Temperature field in mass concrete at early-age: Experimental research and numerical simulation," *Int. J. Emerg. Technol.*, vol. 11, no. 3, 2020.
- [12] A. M. Lawrence, M. Tia, C. C. Ferraro, and M. Bergin, "Effect of Early Age Strength on Cracking in Mass Concrete Containing Different Supplementary Cementitious Materials: Experimental and Finite-Element Investigation," *J. Mater. Civ. Eng.*, vol. 24, no. 4, 2012, doi: 10.1061/(asce)mt.1943-5533.0000389.
- [13] M. K. Saeed, M. H. Baluch, and M. K. Rahman, "Early age thermal cracking of mass concrete blocks with Portland cement and ground granulated blast-furnace slag," *Mag. Concr. Res.*, vol. 68, no. 13, 2016, doi: 10.1680/jmacr.15.00044.
- [14] Z. Zhao, K. Wang, D. A. Lange, H. Zhou, W. Wang, and D. Zhu, "Creep and thermal cracking of ultra-high volume fly ash mass concrete at early age," *Cem. Concr. Compos.*, vol. 99, no. March, pp. 191–202, 2019, doi:

- 10.1016/j.cemconcomp.2019.02.018.
- [15] A. Schindler, B. Byard, and A. Tankasala, "Mitigation of early-age cracking in concrete structures," *MATEC Web Conf.*, vol. 284, 2019, doi: 10.1051/mateconf/201928407005.
- [16] BS-EN 197-1, "Methods of testing Composition, Specifications and Conformity Criteria for Common Cements," *BSI Stand. Publ.*, no. November, p. 50, 2011.
- [17] ncegypt, *CEM I 42.5 N*. [http://www.ncegypt.com/NCCEGYPT.COM/uploads/cms/sahm CEM I 42.5 NRdetails.png](http://www.ncegypt.com/NCCEGYPT.COM/uploads/cms/sahm%20CEM%20I%2042.5%20NRdetails.png).
- [18] D. S. Atrushi, "Tensile and Compressive Creep of Early Age Concrete : Testing and Modelling," *Sci. Technol.*, no. 3377, 2003.
- [19] S. Zhao, X. Ding, M. Zhao, C. Li, and S. Pei, "Experimental study on tensile strength development of concrete with manufactured sand," *Constr. Build. Mater.*, vol. 138, 2017, doi: 10.1016/j.conbuildmat.2017.01.093.
- [20] C. keun Lim, J. K. Kim, and T. S. Seo, "Prediction of concrete adiabatic temperature rise characteristic by semi-adiabatic temperature rise test and FEM analysis," *Constr. Build. Mater.*, vol. 125, pp. 679–689, 2016, doi: 10.1016/j.conbuildmat.2016.08.072.
- [21] M. A. Ahmed, Y. A. Hassanean, K. A. Assaf, S. I. El-Dek, and M. A. Shawkey, "Piezoelectric response of MWCNTs/cement nanocomposites," *Microelectron. Eng.*, vol. 146, pp. 53–56, 2015, doi: 10.1016/j.mee.2015.03.058.
- [22] A. M. Lawrence, "A finite element model for the prediction of thermal stresses in mass concrete," p. 178, 2009.